Plasma assisted large-scale nanoassembly of metal-insulator bioplasmonic mushrooms

Nikhil Bhalla,* Shivani Sathish, Casey J. Galvin, Robert A. Campbell, Abhishek Sinha, and Amy Q. Shen*

Micro/Bio/Nanofluidics Unit, Okinawa Institute of Science and Technology Graduate School, 1919-1 Tancha, Onna-son, Okinawa, 904-0495, Japan

E-mail: nikhil.bhalla@oist.jp; amy.shen@oist.jp

Abstract

Large-scale plasmonic substrates consisting of metal-insulator nanostructures coated with a bio-recognition layer can be exploited for enhanced label-free sensing, by utilizing the principle of localized surface plasmon resonance (LSPR). Most often the uniformity and thickness of the bio-recognition layer determines the sensitivity of plasmonic resonances as the inherent LSPR sensitivity of nanomaterials is limited to 10–20 nm from the surface. However, due to time-consuming nanofabrication processes, there is limited work on both the development of large-scale plasmonic materials, and the subsequent surface functionalizing with bio-recognition layers. In this work, by exploiting properties of reactive ions in a SF_6 plasma environment, we are able to develop a nanoplasmonic substrate containing $\sim 10^6/\text{cm}^2$ mushroom-like structures on a large sized silicon dioxide substrate (i.e., 2.5 cm by 7.5 cm). We further investigate the underlying mechanism of the nanoassembly of gold on glass inside the plasma environment, which can be expanded to a variety of metal-insulator systems. By incorporating a novel microcontact printing technique, we deposit a highly uniform bio-recognition layer of proteins on the nanoplasmonic substrate. The bioplasmonic assays

performed on these substrates achieve a limit of detection of 10^{-17} g/mL ($\sim$ 66 zM) for biomolecules such as antibodies ($\sim$ 150 kDa). Our simple nanofabrication procedure opens new opportunities in fabricating versatile bioplasmonic materials for a wide range of biomedical and sensing applications.

Keywords

nanophotonics, microcontact-printing, nanomushrooms, plasma, nanoassembly

1 Introduction

Constituting a major class of photonic nanomaterials, nanoplasmonic materials are made of nanostructures where the electron density of the material can be coupled with electromagnetic radiation of wavelengths that are greater than the size of the nanostructure. These materials are not only important for the development of fundamental knowledge in quantum mechanics and optics, but also as a foundation for enabling technologies related to biosensors, telecommunication devices, solar cells, light-emitting diodes, video processing and imaging systems.[1–3] One fundamental principle associated with noble metal nanoplasmonic structures is localized surface plasmon resonance (LSPR).[4–6] LSPR is the coherent oscillation of the surface electrons of metal nanostructures due to interactions between the incident light and the conduction band electrons of the metal.[7,8] LSPR technology has been utilized to perform highly sensitive label-free detection of biomolecular interactions in real time, an essential feature for the early detection of diseases and point-of-care (POC) clinical evaluations.[1,8,9] However, standardized LSPR technology for routine clinical evaluations is still lacking due to challenges in fabricating nanoplasmonic materials on large scale substrates.[10,11]

Two fundamental fabrication methodologies are routinely used to manufacture nanoplasmonic materials: top-down fabrication and bottom-up assembly.[12] Top-down fabrication typically relies on various lithographic methods,[13] whereas bottom-up approaches employ

molecular and polymer templating,[14,15] and colloidal chemistry[16] to develop structures with nanometer dimensions.[13] Although the inherent nature of the bottom-up approach enables fine resolution, top-down methods are better suited for large-scale, high-throughput nanostructure production.[12,17] For example, various lithograhy techniques such as e-beam lithography,[18] angled-nanospherical lens[19] and conventional photolithography[20] have been employed to fabricate large-scale nanoplasmonic substrates, for subsequent applications in spectroscopy[21] and large-scale communication devices.[22] However, most often lithography techniques involve time consuming steps to fabricate nanostructures at large scale. Existing techniques to fabricate nanoplasmonic structures on large scale substrates also have limitations.[23–25] For instance, the performance of nanoimprint lithography can be affected by the density of precursor particles.[26] Other technologies such as X-ray interference lithography and UV lithography,[26,27] though lower in cost and allowing the fabrication of nanostructures in large areas, suffer from low resolutions. Utilizing the merits of both top-down and bottom-up approaches has seen some success in developing polymeric and small-scale metal-dielectric materials. For instance, Molnár *et al.* developed a combined top-down bottom-up approach to fabricate 3D polymer structures at nanoscale.[17] Additionally, Choi *et al.* deposited gold nanostructures on silicon by combining photolithography, deposition and etching steps.[28] Baquedano *et al.* developed a hybrid method of using soft lithography patterning with plasma etching to fabricate large scale plasmonic optical gratings (355 nm wide with a period of 780 nm).[29] Such nanostructures are easy to fabricate in large areas, but due to the low surface to volume ratio, these gratings are not suitable for sensing biomolecules at ultra-low concentrations (sub-picomolar). Moreover, the large inter-nanostructure spacing makes the sensing surface more prone to non-specific biomolecule adsorption.

Motivated by this challenge, we develop a combined top-down/bottom-up approach to create large-scale gold (Au) nanoplasmonic structures with high-throughput production. Our process utilizes properties of reactive ion environments (plasma) of SF_6 to assemble gold nanomushroom-like structures. The gas plasma environment has been reported to as-

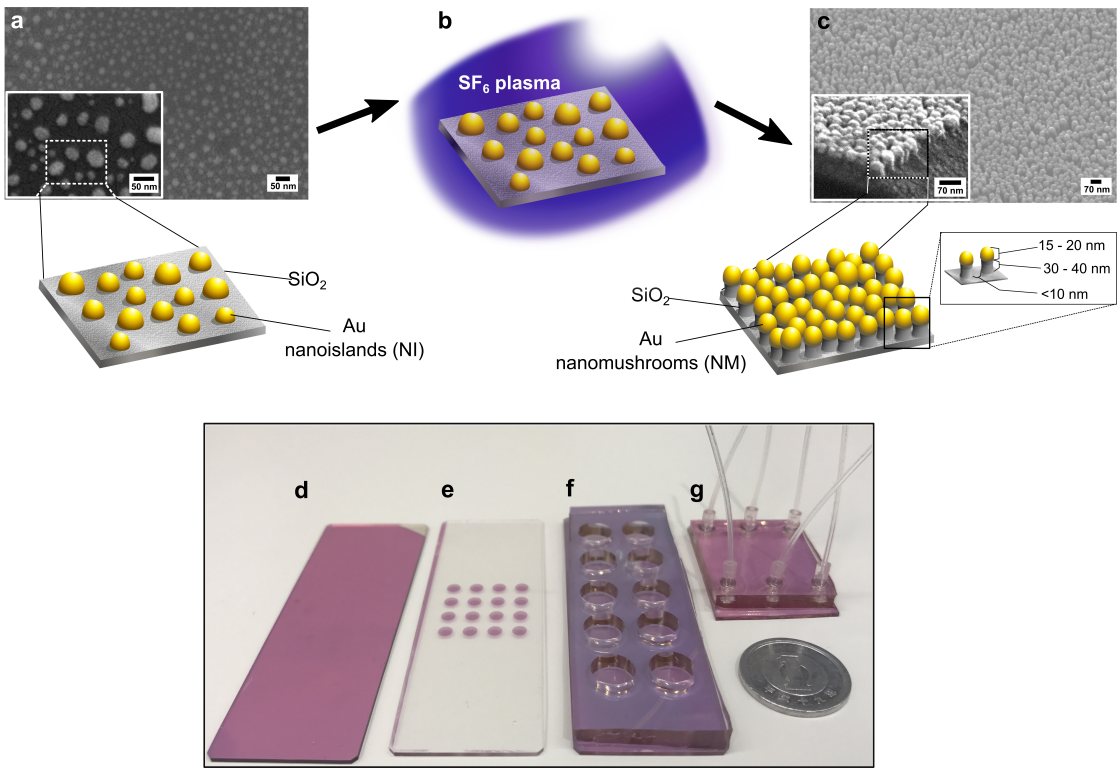

Figure 1: **Transforming Au Nanoisland (NI) precursors to nanomushroom (NM) arrays in SF_6 plasma:** a) Scanning electron microscopy (SEM) image (Quanta 250 FEG, 5 KV, 100 kX magnification) and schematic of NIs. b) Schematic showing a SiO_2 substrate with NIs inside a SF_6 plasma chamber, where SF_x reactive ions etch out both SiO_2 and Au. c) SEM image and schematic of NMs formed after exposure to reactive ion etching inside SF_6 plasma. The inset shows the cross section of the NMs. The developed NM structures are 45–60 nm in total height with an average spacing of 7.96 ± 2.12 nm. Examples of various configurations of NM substrates or integrated chips: d) NM coated glass slide of size 2.5 cm × 7.5 cm. The pink color corresponds to the Au nanostructures; e) Spots of 3 mm circles for multiplex bioassay applications; f) Integrating PDMS wells on a NM substrate; g) Sealed device with PDMS microfluidic channels on a NM substrate, connected with liquid delivery tubings. One Japanese yen coin (∼ 20 mm in diameter) serves as a scale.

sist in deterministic nanofabrication for polymeric, silicons and carbon-based materials.[30] However, this is the first attempt to exploit properties of a plasma environment to develop nanoplasmonic substrates containing mushroom-like Au-topped nanostructures on a large silicon dioxide (SiO_2) substrate (2.5 cm×7.5 cm), as shown in Figure 1. Briefly, a 4 nm thin layer of Au was deposited on a SiO_2 surface. The Au thin films were then annealed at 560 °C to produce nanoisland (NI) like structures of Au. Nanomushrooms (NMs) were then formed by exposing the NI decorated SiO_2 substrate to a low-temperature (5 °C) plasma of

sulfur hexafluoride (SF_6) gas. Ions of SF_6 selectively etched off SiO_2, while Au NIs served as nanomasks for the underlying SiO_2. This masking resulted in the formation of NM structures, where each NM consists of a SiO_2 stem of 30–40 nm in height, and a Au cap of 15–20 nm in thickness, evenly distributed with 7.96 $\pm$ 2.12 nm spacing (see Figure 1c). The fabricated NM nanoplasmonic substrate was then used as an LSPR chip (see images in Figure 1(d-g)) and characterized for generic bioassay applications for protein binding studies. The bio-recognition layer containing the primary antibodies was immobilized on the substrates by using microcontact printing techniques. The homogeneous nanomushroom morphology allowed us to create more uniform protein coating on NM based LSPR chip. The bioplasmonic assay performed on these substrates achieved a limit of detection of $\sim$ 66 zM for biomolecules such as antibodies ($\sim$ 150 kDa).

2 Experiments

2.1 Nanomushroom (NM) fabrication process

Nanolayers of Au were deposited on SiO_2 using an electron beam vapor deposition equipment (KE604TT1–TKF1, Kawasaki Science) in a class 1000 clean room. The substrates were cleaned with acetone and isopropanol before deposition. A 4 nm Au film was deposited at a rate of 0.3 nm/sec. The sample was then annealed at 560 °C for 3 hours, generating a distribution of Au NIs across the surface of the substrate. An inductively coupled plasma chemical vapor deposition (ICP CVD) equipment (Plasmalab 100, Oxford Instruments) was then used to perform reactive ion etching (RIE) on the sample containing Au NIs. SF_6 gas was introduced inside the RIE chamber, maintained at an inside pressure of 10 mtorr and a flow rate of 45 sccm (Standard Cubic Centimeters per Minute). The RF power coil and the RF bias coils were fixed to 150 W and 10 W respectively and the temperature inside the plasma chamber was maintained at 5 °C. The total duration of RIE was 5 minutes.

2.2 Electron beam lithography

Electron beam lithography (EBL) was used to fabricate a series of uniformly-sized Au NI arrays with 200 nm in diameter and 100 nm in spacing. EBL was performed on Si wafers with a thin (10 nm) layer of natural oxide, and on Si wafers coated in a more robust, 500 nm layer of SiO_2. Samples were spin coated with the positive e-beam resist AR-P 6200 at 500 rpm for 10 seconds, followed by 6000 rpm for 50 seconds. They were then soft baked at 150 °C for 3 minutes. EBL was performed at 10 pA with a field size of 150 nm, and with the arrays replicated 16 times in a pixel exposure series of 0.8–1.55 s. Development of the EBL patterns was performed for 30 seconds in amyl acetate before being washed in IPA.

2.3 Material characterizations

A small section of the substrate was cut from the original sample using a diamond-tipped glass cutter and attached to a scanning electron microscope (SEM, FEI Quanta 250 FEG) mount using carbon tapes. SEM measurements were taken between 5–30 eV to obtain high resolution images with magnification of at least 100 kX.

2.4 LSPR instrumentation and measurements

The instrument used to study LSPR response was custom assembled by combining discrete optical components necessary for illumination and collection of light from the sample. The setup is similar to the setups used in our prior work.[31] Briefly, the assembly involves a 2 fibre optics patch cords , one connected with a halogen light source (LS-1-LL) and other connected to a spectroscope (USB4000-UV-VIS-ES), which were all purchased from Ocean Optics. The fibre optics were alligined for light exposure and collection of light in transmission setup using RTL-T stage purchased from Ocean Optics. Before taking any signal from the spectroscope, the system was calibrated for dark and light spectrum modes. The LSPR signal was then recorded in absorption mode by observing the wavelength dependence of the

light absorbed by nanostructures via the OceanView software (cross-platform spectroscopy operating software from Ocean Optics).

2.5 Microcontact printing and bioassay

PDMS (Polydimethylsiloxane) stamps comprising of (i) an array of 50 μm×50 μm squares with 50 μm spacing; (ii) the logo of the university (50 μm in thickness with a total diameter of 1 mm), were designed with AutoCAD (AutoDesk, USA). To fabricate the master for the stamps, silicon wafers (4-inch in diameter, EM Corp. Ltd., Japan) were coated with a 50 μm layer of mr-DWL 40 photoresist (Microresist technologies, Germany), and the features were patterned by photolithography using a DL1000 maskless writer (NanoSystem Solutions, Japan), and developed using mr-Dev 600 developer (Microresist Technologies, Germany). After thorough baking and cleaning, the wafers were coated with an anti-adhesive layer by exposing it to trichloro(1H, 1H, 2H 2H-perfluorooctyl) silane (Sigma-Aldrich, Japan) in vapor phase in a desiccator. PDMS stamps with the inverse copy of the pattern present on the Si-wafer were obtained by pouring 10:1 (base to crosslinker) PDMS mixing ratio (DOW Corning, Japan) on the wafer and curing the pre-polymer for 24 h at 60 °C after degassing to remove air bubbles.

Prior to the microcontact printing process, the Au NIs and NMs covered SiO_2 substrates were cleaned with ethanol and dried well. The patterned stamps were inked with 10 μL of AlexaFluor 546-conjugated goat anti-chicken immunoglobulins (IgGs) (Abcam, Japan) at a concentration of 10 μg/mL in 1×PBS, for 5–7 minutes under a plasma activated (Harrick Plasma, USA) coverslip. The stamps were rinsed with 1×PBS followed by milli-Q water (Millipore, Japan) for 5 s each before rapid drying with a strong pulse of N_2 gas. The inked PDMS stamps were then contacted with pre-cleaned substrates for 5 s. Subsequently, the micropatterns of the fluorescently labeled IgGs were imaged on a Ti-E Eclipse inverted fluorescent microscope (Nikon, Japan) with a fixed exposure time of 10 s for all samples. After confirming the presence of printed capture IgGs, the patterned IgGs were exposed to

varied concentrations of AlexaFluor 488-conjugated chicken anti-goat IgGs (Abcam, Japan) for dose-response bioassay studies.

3 Results and Discussions

3.1 Fabrication and nanoassembly mechanism

Au NIs shown in Figure 1a and Figure 2(a(i), b, d), were created by depositing a 4 nm layer of Au onto a SiO_2 surface by electron beam vapor (e-beam) deposition, after which the structures were annealed at 560 °C for 3 hours. The process of annealing ruptured the thin Au film deposited on the SiO_2 substrate into island-like structures as a result of the Au film dewetting.[32] Previous work has used the dewetting of Au on glass to submerge Au nanoparticles into glass substrates to fabricate nanochannels[33] and nanoislands.[34] Our annealing temperature is lower than the reported work, which is why Au NIs stay on the SiO_2 surface. However, we cannot rule out that the Au/glass interface is not affected by the annealing process.

Next, the SiO_2 substrate containing Au NIs was subjected to RIE in a SF_6 plasma environment at 5 °C for 5 minutes, with Au NIs serving as nanomasks for the SiO_2 substrate, see schematic in Figure 2a(i–iv) highlighting each key step. SF_6 gas etched SiO_2, as the SiO_2 around each NI was removed. SF_6 etching of SiO_2 is a well-established process, and usually involves (1) generation of reactive fluorine species (SF_x), (2) diffusion of these species to the SiO_2 surface and subsequent adsorption on the SiO_2 surface, (3) reaction with SiO_2, both chemically and physically (such as sputtering), (4) desorption and (5) diffusion of reaction products into the bulk gas.[35,36] In parallel, Au NIs were also etched from the surface by both physical and chemical processes. However, SF_6 etches Au at rates approximately 100 times slower than that of the etching of SiO_2.[37] The physical etching processes, such as sputtering, was primarily due to the bombardment of negative SF_x ions that were accelerated toward the substrate by strong electric fields,[38] whereas chemical reaction of Au with SF_6 generated

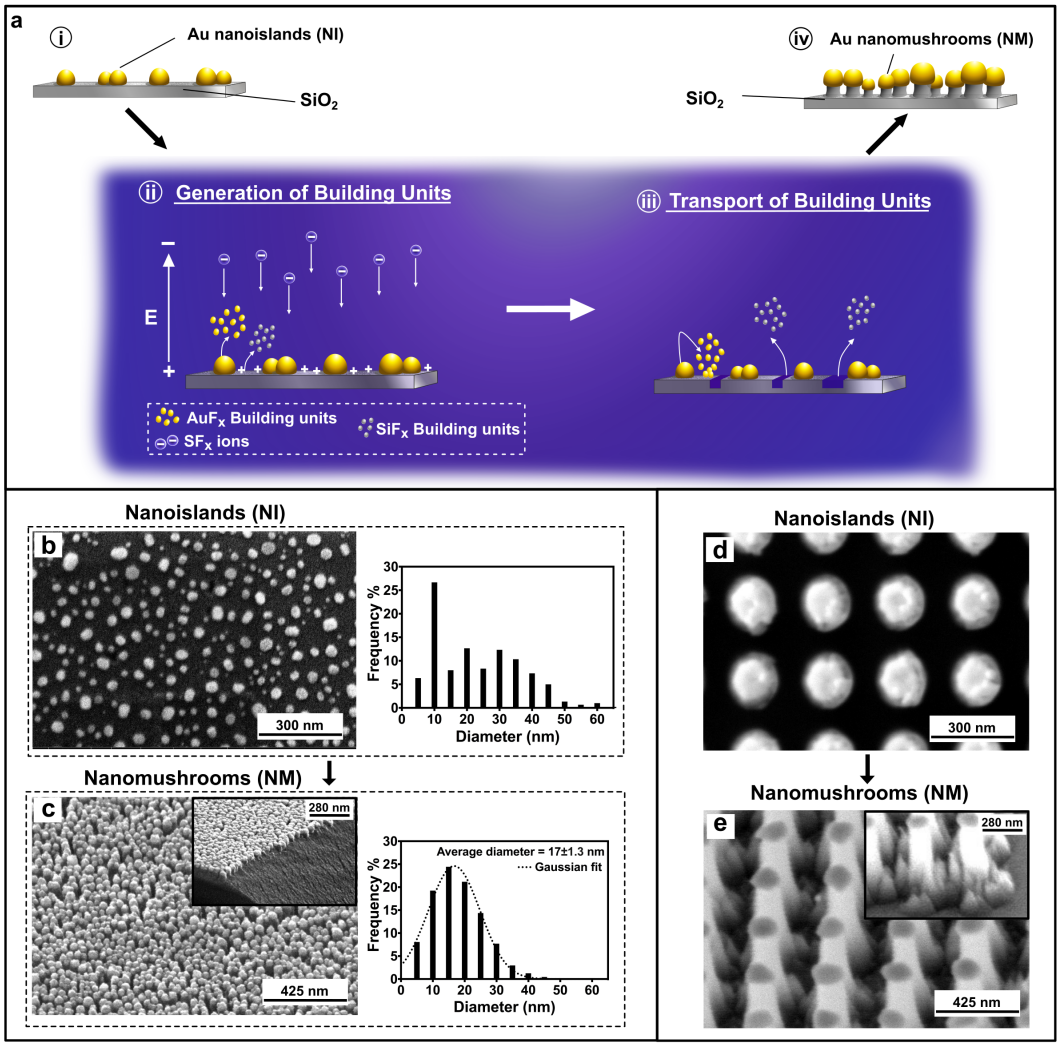

Figure 2: **Fabrication process to form nanomushroom-like structures (NMs).** a) Schematic illustrates (i,ii) the generation of building units from Au nanoislands (NIs), and (iii,iv) subsequent transport and assembly of building units into more tightly packed NMs under RIE in a SF_6 plasma chamber; Scanning electron microscopy (SEM) images (Quanta 250 FEG, 5KV, 100 kX magnification) of NIs and NMs; b,c) Transformation of NI arrays, prepared by dewetting process with heterogeneous size (5-60 nm) and spacing (10–70 nm), to NMs of 45-60 nm in height, 20 nm in diameter, topped with Au cap, with an average spacing of 7.96 ± 2.12 nm. The histograms show the size distribution of NI and NM respectively; d,e) Transformation of ordered NI arrays prepared by e-beam lithography (200 nm in diameter with a spacing of 100 nm) to NMs with 150–200 nm of Au caps. Note there are 2 types of NMs, one formed from the original NIs and other, deposited in the original vacant sites, clearly shown in the inset in (e).

AuF_x species, see Figure 2a(i, ii). These etched off Au entities (in the form of atoms, clusters of atoms and molecules of Au) were thus available to serve as building units for further assembly.[39] In short, the formation of NM was facilitated by: (a) SiO_2 being ejected

from the substrate into the plasma chamber; (b) Au building units being redistributed on the SiO_2 surface to form new Au nanostructures, see Figure 2a(iii). This redistribution of Au building units back on the SiO_2 surface is attributed to the fact that AuF_x species are non-volatile in nature, in comparison to highly volatile SiF_x species generated by the interaction of SF_6 ions with the SiO_2 substrate.[40] These newly deposited Au building units accumulate to form new NIs. Simultaneously, the SiO_2 around the NIs was etched off, resulting in NMs after the RIE process, as shown in Figure 2a(iv).

Further evidence is provided by X-Ray photoelectron spectrometry (XPS) with elemental analysis of the surface of NM, NI and bare glass substrates for the contents of silicon (Si), oxygen (O), gold (Au) and fluorine (F) (see more details in SI). In Figure S1(c, d), the NM substrate displayed stronger peaks of Au and F, after the NI structures were etched off, suggesting that non-volatile AuF_x species fell back on the glass substrate during etching. Simultaneously, there is a substantial increase in the Au 4f signal for the NM, confirming that NMs are capped with gold at higher density. This is consistent with the size distribution difference between the NM and NI substrates depicted by Figure 2(b, c). For instance, the number density of nanosturctures in the NM substrate is significantly higher than those in the NI substrate. Moreover, the average size of the nanostructures in the NM substrate is around 17 ± 1.3 nm, in comparison to heterogeneous distribution of nanostructures in the NI substrate.

We also performed radial distribution function (RDF) analysis of SEM images of NMs to estimate the size and the gap, and further assess the homogeneity of the NM structures (see more details in SI document). Figure S6 shows that the average spacing of NM structures is around 7.96 ± 2.12 nm. Low standard deviation of 4.91% in the average normalized peak intensity from the SEM image implies that the NMs consist of quasi-periodic structures. Given this rather homogenous distribution of NM Au cap size and NM height (see Figure 2c), the reorganization of Au on the surface appears to happen quickly relative to the etching of the glass stems of the NMs.

The non-periodic distribution of the NI precursors fabricated by annealing and dewetting of Au on SiO_2 made it difficult to observe how Au building units were re-deposited on the SiO_2 substrate to form NMs. To support and illustrate our explanation that Au building units are generated from NIs when reacted with SF_6 plasma and re-deposited in the gaps between the NI structures, we designed a well-controlled experiment by creating initial Au NIs with periodic distributions to further investigate the roles and fate of the building units towards the assembly of new NMs. We first fabricated Au NIs (200 nm in diameter and 40 nm in height, with 200 nm spacing) on SiO_2 by using e-beam lithography, and then subjected the substrate to reactive ion etching of SF_6 (same etching time, gas pressure and flow rate as before). In such a case, the location of newly formed NM structures after plasma exposure can be easily tracked based on the original periodic locations of the precursor NIs. As seen in Figure 2(d, e), we were able to observe clearly the newly formed secondary NMs in the original gaps between NIs, upon etching with SF_6 plasma. These observations support our hypothesis that during RIE in plasma, non-volatile AuF_x species build up and re-deposit to vacant sites on the SiO_2 surface. Similarly, the reorganization property of the reactive ions in a plasma environment was recently demonstrated by Levchenko *et al.*, where Nickel (Ni) nanodots were assembled on silicon substrates in a plasma environment with reactive ions of Argon.[41] Note that the experiment shown in Figure 2 (d, e) was carried out only to reveal the generation of building units and their re-deposition, but not used for sensing applications. This is mainly due to the fact that, the dewetting protocol employed to generate NIs for subsequent etching and fabrication of NMs (Figure 2(b, c)) is simpler, less time-consuming and more practical for sensing applications, in comparison to the e-beam lithography method employed to create larger structures of controlled sizes and spacing (Figure 2(d, e)).

We further demonstrate that nanoplasmonic substrates containing Au-SiO_2 NMs are compatible for microcontact printing of proteins and can be used as a novel biosensor for generic bioassay applications. Generic bioassays are commonly characterized by the binding of molecules on a given surface or binding of one molecule to another molecule (such as

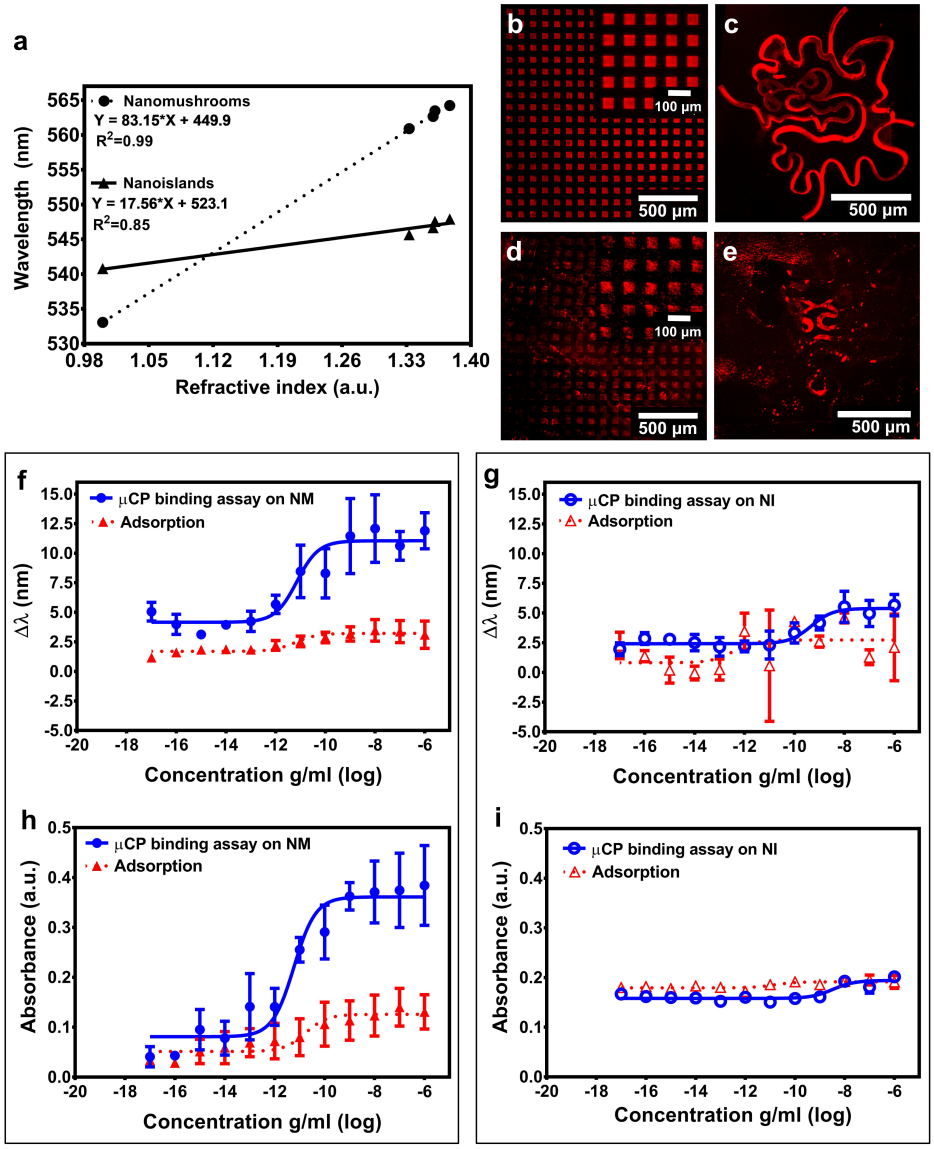

Figure 3: **Characterization of NM substrate for binding assays.** (a) Wavelength is plotted against the refractive index for Au NM and NI substrates when exposed to solutions with different refractive indices: DI-water (1.3330), Acetone (1.3590), Ethanol (1.361) and IPA (1.3776), each point is averaged by measurments from 6 identical samples; Fluorescent IgGs patterned by micro-contact printing in 50 μm×50 μm squares and in the shape of the OIST university logo respectively on Au NM (b & c) and Au NI (d & e). Subfigures (f & g) LSPR wavelength shifts and (h & i) LSPR absorbance shifts for NMs & NIs based nanoplasmonic substrates respectively, to varied amounts of complementary IgGs being attached to the microcontact printed IgGs (blue symbols) and the control reaction (red symbols) on adsorption of complementary IgGs. Comparing figure 3h and i we can observe that NM substrates are more sensitive than NI as NI absorbances do not change as much as the absorbances of NM structrues in response to antibody attachment. Large error bars observed in subfigures f to i are due to varied levels of non-specific attachment of complementary antibodies in areas where no primary antibodies are printed. Note: many points on subfigure 3i do not show error bars as the size of the symbol is larger than the standard deviations.

antibody-antigen interaction). The Au NIs were found to resonate at 540 nm and Au NMs at 533 nm, see Figure S4 in the SI document. In general, decreasing the ratio of width to height of a nanostructure results in blue shifts (decrease) in the wavelength of LSPR.[42,43] Therefore, the wavelength peak shift (blue shift) of 7 nm from Au NMs to Au NIs structures is attributed to 1) smaller average size and narrower distributions in NMs; and 2) increase in electronic charge density due to field enhancement in pillared nanostructures. Figure 3a shows that the changes in the wavelength ($\Delta\lambda$) of Au nanostructures are caused by the change in the local refractive index around the nanostructures. The refractive index of the Au nanoplasmonic substrates (Au NMs and Au NIs) was characterized using water, acetone, isopropanol and ethanol. The slope of the fit provides the sensitivity of the nanostructured substrate: NM substrates are 4 times more sensitive (83.1 nm/RIU) than that of NI substrates (17.5 nm/RIU). The increased periodicity due to the quasi homogeneous distribution of NMs enables the enhancement in sensitivity of NM substrate performances.[44] Furthermore, the tips of Au NMs are much sharper than those of NIs. It is well known that sharp nanostructured features give rise to hot-spots in the electromagnetic field that increase the sensitivity to changes in local refractive index and amplify surface-enhanced phenomena such as LSPR.[45,46] This sensitivity is reasonably good for a large sensor substrate containing spherical gold nanostructures for LSPR applications, with reported range of 20-96 nm/RIU.[47] Moreover, it is possible to improve the sensitivity of the NM substrate by modifying fabrication parameters (such as initial thickness of gold film and time of exposure to plasma) to optimize the NM size, aspect ratio and spacing. This is ascribed to the fact that any changes in NM geometry generally leads to a change in LSPR response. The condition $R/\lambda < 0.1$, where R is the radius of the nanostructure and λ is the wavelength of the incident light, should be satisfied for LSPR.[48] The LSPR sensitivity can be enhanced by reducing the ratio of R/λ, i.e., decreasing the size of the nanostructure with fixed wavelength.[26] The second parameter to consider in our NM geometry is the periodicity of the nanostructures where decreasing the spacing of the nanostructures can also enhance the sen-

sitivity of the LSPR.[49] More systematic studies are required in the future to optimize the size and distribution of NM structures for enhanced sensitivity of the NM based biosensor.

To validate the use of Au NMs for generic bioassay applications, we carried out a proof-of-concept binding study, where AlexaFluor 546-conjugated goat anti-chicken IgGs were chosen as the "capture IgGs" and AlexaFluor 488-conjugated chicken anti-goat IgGs were selected as the "complementary IgGs". To immobilize the capture IgGs onto the Au NI and NM substrates, we exploited the microcontact printing (μCP) technique (more details in the SI document): a simple method that involves transfer of biomolecules from a PDMS stamp onto higher surface energy substrates in controlled microscale features with high accuracy and reproducibility.[50,51] Figure 3(b, c) depict printing of fluorescently-labelled IgGs on Au NMs substrates and Figure 3(d, e) depict printing of fluorescent IgGs on Au NIs substrates, both in well-defined geometries. It is worth noting that the printing of IgGs on NMs substrates is more uniform than on NIs, correlated with more uniform and densely packed NM structures on the SiO_2 substrate (Figure 3(b,c)). A complex pattern (OIST university logo) of IgGs was also successfully printed on NMs (Figure 3c), while a less uniform transfer of antibodies on the Au NIs substrate was achieved (Figure 3e). The importance of patterning surfaces with proteins in 'complex' patterns with uniformity, has been highlighted in cell-behavior studies, as it allows the creation of well controlled micro/nano environments for cell growth.[52] These results stress the utility of plasma assembled large-scale Au NMs as superior nanostructures for sensing and for complex biomolecules patterning.

Subsequently, the complementary IgG pair in solutions with incremented concentrations were deposited to the μCP substrates, until signal saturation was reached. In Figure 3 (f, h), LSPR responses (changes in wavelength and absorbance intensity respectively) for the specific binding of IgGs to its complementary pair patterned on NMs (in blue symbols); and the adsorption of complementary IgGs on blank NM surfaces without patterned antibodies (in red symbols as control) were plotted. A standard bioassay response (S-shaped) was observed against varied concentrations of complementary IgGs in both wavelengths shift

and absorbance intensity shift of the LSPR signal. Upon attachment of 10 ag/mL of complementary IgGs on the patterned NM surface, an average LSPR red shift of ~ 5 nm and less than 0.1 unit of change in absorbance intensity was observed. The LSPR response shows less than ~ 2 nm and ~ 0.1 U change upon further addition of IgGs up to a concentration of ~ 100 fg/mL. Above ~ 100 fg/mL, a dynamic response in the LSPR signal was observed upon addition of IgG concentrations ranging from ~ 100 fg/mL to ~ 100 pg/mL, after which the LSPR signal saturates. Therefore, we consider ~ 100 fg/mL to ~ 100 pg/mL as the dynamic concentration range of our Au NMs LSPR substrate for this particular case study. It must be noted that the dynamic range of the sensor is not an absolute biosensing parameter and it will vary from one analyte to the other.

The LSPR signal variation due to absorbed IgGs showed less than 3 nm and 0.1 U of change in the absorbance characteristics of the LSPR response. These changes were caused by non-specific attachment of IgGs at high concentrations on the NM substrate. The limit of detection (LOD) of the sensor was computed by comparison of standard deviation and mean values of blank/control samples versus the experimental data set[53] (see detailed LOD calculation in SI). The LOD of IgG binding on the functionalized Au NMs was estimated to be 10^{-17} g/mL ($\sim$66 zM). This particular concentration is the lowest concentration of analyte likely to be reliably distinguished from controls and at which detection was feasible. The LOD value of 10^{-17} g/mL can be further asserted by observing wavelength change differences in control (red line) and binding assay (blue line) shown on figure 3f. However, it must be noted that for concentrations between 10 ag/mL and 100 fg/mL there is no significant signal variation within the average. Therefore, in our experiment it is not possible to detect IgG reliably below 100 fg/mL, which we call as the limit of quantification (LOQ) of the sensor. LOQ can be either equal to LOD or higher than LOD. LOQ is generally determined by the user to satisfy imprecisions in theoretical LOD calculations which account for lack of accuracy in LOD models to predict practical sensing limits.[53]

These studies confirm that NM based substrates can be used as a highly sensitive plat-

form for generic bioassay applications and for the detection of biomolecule binding events on patterned surfaces. To further justify the need of NM development, binding assay on NI substrates was carried out for the detection of IgG antibodies. Figure 3(g, i) show LSPR wavelength and absorbance response of NI structures to varied (10^{-17} to 10^{-6} g/mL) concentrations of IgG complimentary antibodies. We observed less than 7 nm of shifts in the wavelength response of NIs (Figure 3g) as compared to over 13 nm of wavelength shifts on NMs substrates (Figure 3f). Furthermore, the wavelength changes on NIs can not be distinguished from the adsorption assay, suggesting that the results shown in NIs were caused by non-specific binding. Similarily, the absorbance response of NIs is also not distinguishable from the adsorption control (Figure 3i). These results suggest that NMs are superior to NIs substrates for biosensing applications. The LSPR binding curves for both NMs and NIs substrates are shown in Figure S4, in SI document.

Conclusion

In summary, we developed a simple nanofabrication protocol for generation of Au-SiO_2 nao-mushroom structures, and provided insights on the potential mechanisms that exploit the assembly of metal at nanoscale in a plasma environment. The effects of SF_6 plasma lead to localization and control of energies at nanoscales, producing organized Au NMs with superior properties for sensing applications. Our NM substrates were able to detect proteins down to zepto molar concentrations as they allow uniform printing of capture antibodies on their surfaces. Moreover, the fabrication process can be extended to other nanostructured metals by proper operating combinations of reactive ions, gas pressures and etching rates. Further, plasma assisted metal species assembly provides an effective manufacturing route for the production of stable nanostructures on substrates with large surface areas. Our nanofabrication technique presents an attractive platform in the development of cost effective fabrication processes for plasmonic biosensors. Significantly, this process is 'scal-

able', as the size of the NM substrate is proportional to the size of the thin film evaporator and furnace, readily available at most nanofabrication facilities whose sizes can always be tailored according to the need. With this important feature, the described plasma-assisted nanofabrication process offers immense opportunities to transfer nanoplasmonic substrate fabrication technology from the laboratory to industry and clinical settings.

Supporting Information Available

The following files are available free of charge.

One file consisting following information:

- X-Ray photoelectron spectrometry (XPS) characterizations on Au NMs, Au NIs, and bare glass substrates for silicon (Si), oxygen (O), gold (Au) and fluorine (F) contents.
- LSPR characteristic curves of Au NIs and NMs substrates.
- Limit of detection (LOD) calculations of Au NMs substrates.
- Microcontact printing process of proteins.
- Binding assay and concentration dependent dose response on Au NMs and NIs substrates.
- Structural analysis of Au NMs: radial distribution analysis

Acknowledgement

We gratefully acknowledge support from OIST Graduate University with subsidy funding from the Cabinet Office, Government of Japan. In particular the work was supported by the OIST Proof of Concept grant. Authors would like to thank Mr. Laszlo Szikszai and

Dr. Alexander Badrutdinov from OIST for their help with the e-beam lithography and reactive ion etching respectively. We would like to thank Dr. Francesco Del Giudice for useful discussions during the course of this work.

References

(1) Sreekanth, K. V.; Alapan, Y.; ElKabbash, M.; Ilker, E.; Hinczewski, M.; Gurkan, U. A.; De Luca, A.; Strangi, G. Extreme sensitivity biosensing platform based on hyperbolic metamaterials. *Nature Materials* **2016**, *15*, 621.

(2) Limaj, O.; Etezadi, D.; Wittenberg, N. J.; Rodrigo, D.; Yoo, D.; Oh, S.-H.; Altug, H. Infrared plasmonic biosensor for real-time and label-free monitoring of lipid membranes. *Nano Letters* **2016**, *16*, 1502–1508.

(3) Liu, N.; Guo, H.; Fu, L.; Kaiser, S.; Schweizer, H.; Giessen, H. Three-dimensional photonic metamaterials at optical frequencies. *Nature Materials* **2008**, *7*, 31–37.

(4) Anker, J. N.; Hall, W. P.; Lyandres, O.; Shah, N. C.; Zhao, J.; Van Duyne, R. P. Biosensing with plasmonic nanosensors. *Nature Materials* **2008**, *7*, 442–453.

(5) Hammond, J. L.; Bhalla, N.; Rafiee, S. D.; Estrela, P. Localized surface plasmon resonance as a biosensing platform for developing countries. *Biosensors* **2014**, *4*, 172–188.

(6) Szunerits, S.; Boukherroub, R. Sensing using localised surface plasmon resonance sensors. *Chemical Communications* **2012**, *48*, 8999–9010.

(7) Brolo, A. G. Plasmonics for future biosensors. *Nature Photonics* **2012**, *6*, 709–713.

(8) Willets, K. A.; Van Duyne, R. P. Localized surface plasmon resonance spectroscopy and sensing. *Annu.Rev.Phys.Chem.* **2007**, *58*, 267–297.

(9) Dutta, S.; Saikia, K.; Nath, P. Smartphone based LSPR sensing platform for bioconjugation detection and quantification. *RSC Advances* **2016**, *6*, 21871–21880.

(10) Gao, P.; He, J.; Zhou, S.; Yang, X.; Li, S.; Sheng, J.; Wang, D.; Yu, T.; Ye, J.; Cui, Y. Large-area nanosphere self-assembly by a micro-propulsive injection method for high throughput periodic surface nanotexturing. *Nano Letters* **2015**, *15*, 4591–4598.

(11) Lin, Q.; Sarkar, D.; Lin, Y.; Yeung, M.; Blankemeier, L.; Hazra, J.; Wang, W.; Niu, S.; Ravichandran, J.; Fan, Z.; Rehan, K. Scalable indium phosphide thin-film nanophotonics platform for photovoltaic and photoelectrochemical devices. *ACS Nano* **2017**, *11*, 5113–5119.

(12) Xia, Y.; Whitesides, G. M. Soft lithography. *Annual Review of Materials Science* **1998**, *28*, 153–184.

(13) Whitesides, G. M.; Kriebel, J. K.; Mayers, B. T. *Nanoscale Assembly*; Springer, 2005; pp 217–239.

(14) Stender, C. L.; Odom, T. W. Chemical nanofabrication: a general route to surface-patterned and free-standing transition metal chalcogenide nanostructures. *Journal of Materials Chemistry* **2007**, *17*, 1866–1869.

(15) Xianzi, D.; Zhensheng, Z.; Xuanming, D. Improving spatial resolution and reducing aspect ratio in multiphoton polymerization nanofabrication. *Applied Physics Letters* **2008**, *92*, 091113:1–3.

(16) Zhang, J.; Li, Y.; Zhang, X.; Yang, B. Colloidal Self-Assembly Meets Nanofabrication: From Two-Dimensional Colloidal Crystals to Nanostructure Arrays. *Advanced Materials* **2010**, *22*, 4249–4269.

(17) Molnár, G.; Cobo, S.; Real, J. A.; Carcenac, F.; Daran, E.; Vieu, C.; Bousseksou, A. A Combined Top-Down/Bottom-Up Approach for the Nanoscale Patterning of Spin-Crossover Coordination Polymers. *Advanced Materials* **2007**, *19*, 2163–2167.

(18) Staude, I.; Decker, M.; Ventura, M. J.; Jagadish, C.; Neshev, D. N.; Gu, M.; Kivshar, Y. S. Hybrid High-Resolution Three-Dimensional Nanofabrication for Metamaterials and Nanoplasmonics. *Advanced Materials* **2013**, *25*, 1260–1264.

(19) Chien, Y.-H.; Wang, C.-H.; Liu, C.-C.; Chang, S.-H.; Kong, K. V.; Chang, Y.-C. Large-Scale Nanofabrication of Designed Nanostructures Using Angled Nanospherical-Lens Lithography for Surface Enhanced Infrared Absorption Spectroscopy. *ACS Applied Materials & Interfaces* **2017**, *9*, 24917–24925.

(20) Odebo Lank, N.; Verre, R.; Johansson, P.; Kall, M. Large-scale silicon nanophotonic metasurfaces with polarization independent near-perfect absorption. *Nano Letters* **2017**, *17*, 3054–3060.

(21) Scarabelli, L.; Coronado-Puchau, M.; Giner-Casares, J. J.; Langer, J.; Liz-Marzán, L. M. Monodisperse gold nanotriangles: size control, large-scale self-assembly, and performance in surface-enhanced Raman scattering. *ACS Nano* **2014**, *8*, 5833–5842.

(22) Sun, J.; Timurdogan, E.; Yaacobi, A.; Hosseini, E. S.; Watts, M. R. Large-scale nanophotonic phased array. *Nature* **2013**, *493*, 195–199.

(23) Sun, L.; Hu, X.; Wu, Q.; Wang, L.; Zhao, J.; Yang, S.; Tai, R.; Fecht, H.-J.; Zhang, D.-X.; Wang, L.-Q.; Jiang, J.-Z. High throughput fabrication of large-area plasmonic color filters by soft-X-ray interference lithography. *Optics Express* **2016**, *24*, 19112–19121.

(24) McKeating, K. S.; Couture, M.; Dinel, M.-P.; Garneau-Tsodikova, S.; Masson, J.-F. High throughput LSPR and SERS analysis of aminoglycoside antibiotics. *Analyst* **2016**, *141*, 5120–5126.

(25) Xie, L.; Yan, X.; Du, Y. An aptamer based wall-less LSPR array chip for label-free and high throughput detection of biomolecules. *Biosensors and Bioelectronics* **2014**, *53*, 58–64.

(26) Mazzotta, F.; Höök, F.; Jonsson, M. P. High throughput fabrication of plasmonic nanostructures in nanofluidic pores for biosensing applications. *Nanotechnology* **2012**, *23*, 415304:1–7.

(27) Wang, L.; Schift, H.; Gobrecht, J.; Ekinci, Y.; Kristiansen, P. M.; Solak, H. H.; Jefimovs, K. High-throughput fabrication of compact and flexible bilayer nanowire grid polarizers for deep-ultraviolet to infrared range. *Journal of Vacuum Science & Technology B, Nanotechnology and Microelectronics: Materials, Processing, Measurement, and Phenomena* **2014**, *32*, 031206:1–5.

(28) Choi, W. K.; Liew, T. H.; Chew, H. G.; Zheng, F.; Thompson, C. V.; Wang, Y.; Hong, M. H.; Wang, X. D.; Li, L.; Yun, J. A combined top-down and bottom-up approach for precise placement of metal nanoparticles on silicon. *Small* **2008**, *4*, 330–333.

(29) Baquedano, E.; González, M.; Paniagua-Domínguez, R.; Sánchez-Gil, J.; Postigo, P. Low-cost and large-size nanoplasmonic sensor based on Fano resonances with fast response and high sensitivity. *Optics Express* **2017**, *25*, 15967–15976.

(30) Ostrikov, K. Colloquium: Reactive plasmas as a versatile nanofabrication tool. *Reviews of Modern Physics* **2005**, *77*, 489–511.

(31) Bhalla, N.; Lee, D.; Sathish, S.; Shen, A. Q. Dual-mode refractive index and charge sensing to investigate complex surface chemistry on nanostructures. *Nanoscale* **2017**, *9*, 547–554.

(32) Sachan, P.; Kulkarni, M.; Sharma, A. Hierarchical micro/nano structures by combined self-organized dewetting and photopatterning of photoresist thin films. *Langmuir* **2015**, *31*, 12505–12511.

(33) de Vreede, L. J.; van den Berg, A.; Eijkel, J. C. Nanopore fabrication by heating Au particles on ceramic substrates. *Nano Letters* **2015**, *15*, 727–731.

(34) Jia, K.; Bijeon, J. L.; Adam, P. M.; Ionescu, R. E. Sensitive localized surface plasmon resonance multiplexing protocols. *Analytical Chemistry* **2012**, *84*, 8020–8027.

(35) Park, J.; Lee, N.-E.; Lee, J.; Park, J.; Park, H. Deep dry etching of borosilicate glass using SF6 and SF6/Ar inductively coupled plasmas. *Microelectronic Engineering* **2005**, *82*, 119–128.

(36) Knizikevicius, R. Simulations of Si and SiO2 Etching in SF6 + O2 Plasma. *Acta Physica Polonica, A.* **2010**, *117*, 478–483.

(37) Seeger, K.; Palmer, R. Fabrication of silicon cones and pillars using rough metal films as plasma etching masks. *Applied Physics Letters* **1999**, *74*, 1627–1629.

(38) Coburn, J.; Winters, H. F. Ion-and electron-assisted gas-surface chemistryAn important effect in plasma etching. *Journal of Applied Physics* **1979**, *50*, 3189–3196.

(39) Ostrikov, K. *Plasma nanoscience: Basic Concepts and Applications of Deterministic Nanofabrication*; John Wiley & Sons, 2008.

(40) Kang, T. Y.; Kim, G.; Cho, I. H.; Seo, D.; Hong, S. J. Process optimization of CF 4/Ar plasma etching of Au using I-optimal design. *Thin Solid Films* **2009**, *517*, 3919–3922.

(41) Levchenko, I.; Ostrikov, K.; Diwan, K.; Winkler, K.; Mariotti, D. Plasma-driven self-organization of Ni nanodot arrays on Si (100). *Applied Physics Letters* **2008**, *93*, 183102:1–3.

(42) Becker, J.; Trügler, A.; Jakab, A.; Hohenester, U.; Sönnichsen, C. The optimal aspect ratio of gold nanorods for plasmonic bio-sensing. *Plasmonics* **2010**, *5*, 161–167.

(43) Paivanranta, B.; Merbold, H.; Giannini, R.; Buchi, L.; Gorelick, S.; David, C.; Loffler, J. F.; Feurer, T.; Ekinci, Y. High aspect ratio plasmonic nanostructures for sensing applications. *ACS Nano* **2011**, *5*, 6374–6382.

(44) Parsons, J.; Hendry, E.; Burrows, C. P.; Auguié, B.; Sambles, J. R.; Barnes, W. L. Localized surface-plasmon resonances in periodic nondiffracting metallic nanoparticle and nanohole arrays. *Physical Review B* **2009**, *79*, 073412:1–4.

(45) Abbas, A.; Tian, L.; Morrissey, J. J.; Kharasch, E. D.; Singamaneni, S. Hot Spot-Localized Artificial Antibodies for Label-Free Plasmonic Biosensing. *Advanced Functional Materials* **2013**, *23*, 1789–1797.

(46) Sepúlveda, B.; Angelomé, P. C.; Lechuga, L. M.; Liz-Marzán, L. M. LSPR-based nanobiosensors. *Nano Today* **2009**, *4*, 244–251.

(47) Chen, H.; Kou, X.; Yang, Z.; Ni, W.; Wang, J. Shape-and size-dependent refractive index sensitivity of gold nanoparticles. *Langmuir* **2008**, *24*, 5233–5237.

(48) Petryayeva, E.; Krull, U. J. Localized surface plasmon resonance: nanostructures, bioassays and biosensinga review. *Analytica Chimica Acta* **2011**, *706*, 8–24.

(49) Si, G.; Zhao, Y.; Lv, J.; Lu, M.; Wang, F.; Liu, H.; Xiang, N.; Huang, T. J.; Danner, A. J.; Teng, J.; Liu, Y. J. Reflective plasmonic color filters based on lithographically patterned silver nanorod arrays. *Nanoscale* **2013**, *5*, 6243–6248.

(50) Renault, J. P.; Bernard, A.; Juncker, D.; Michel, B.; Bosshard, H. R.; Delamarche, E. Fabricating microarrays of functional proteins using affinity contact printing. *Angewandte Chemie* **2002**, *114*, 2426–2429.

(51) Sathish, S.; Ricoult, S. G.; Toda-Peters, K.; Shen, A. Q. Microcontact printing with aminosilanes: creating biomolecule micro-and nanoarrays for multiplexed microfluidic bioassays. *Analyst* **2017**, *142*, 1772–1781.

(52) Chen, C. S.; Mrksich, M.; Huang, S.; Whitesides, G. M.; Ingber, D. E. Micropatterned surfaces for control of cell shape, position, and function. *Biotechnology Progress* **1998**, *14*, 356–363.

(53) Armbruster, D. A.; Pry, T. Limit of blank, limit of detection and limit of quantitation. *Clin Biochem Rev* **2008**, *29*, S49–52.